The International Journal of Advanced Manufacturing Technology (2018) 95:3013–3028
https://doi.org/10.1007/s00170-017-1441-4

ORIGINAL ARTICLE

Fabrication of serpentine micro-channels on glass by ultrasonic machining using developed micro-tool by wire-cut electric discharge machining

Sankha Shuvra Das[1] · Promod Kumar Patowari[1]

Received: 25 April 2016 / Accepted: 27 November 2017 / Published online: 3 December 2017

Abstract
A rapid method for fabrication of micro-channel on glass substrates is introduced and investigated in this paper. Wire-cut electro discharge machining (WEDM) and ultrasonic machining (USM) were used as manufacturing processes for machining the micro-tools and micro-channels, respectively. The copper micro-tool was machined using WEDM and the optimal design of the tool was achieved using Taguchi design of experiment. After overall evaluation criteria (OEC) analysis, the optimum conditions were achieved as T_{on} as 25 μs, T_{off} as 6 μs, I_p as 1 A, and W_f as 75 mm/s. Further, it was used for fabrication of micro-tools with different profiles such as square, circular, and zigzag. The fabricated micro-tools were used to machine serpentine micro-channels on glass using USM at various power ratings such as 40, 50, and 60%. After machining, net overcut of the micro-channels were found as 74.65, 75.86, and 81.75 μm for square, circular, and zigzag profiles, respectively.

Keywords Micro-channel · Micro-tool · Wire-cut electro discharge machining (WEDM) · Ultrasonic machining (USM)

1 Introduction

Micro-fluidics is becoming one of the evolving areas of research from the last few years. In this field, promising research is going on to investigate a cost-effective and quick method for fabrication of micro-fluidic devices with different materials such as PMMA, PDMS, silicon, glass [1–3] etc. Among them, fabrication of micro-channel on glass substrate is becoming a major interest of research as it can be used for fabrication of many optical detection micro-fluidic devices, which may be used for many bio-chemical or bio-medical applications [4]. Glass-based MEMS or Lab-on-chip devices are more popular because of its better thermal stability, chemical stability, less susceptibility to heat as well as chemical environment, better electrical insulation properties, low cost etc. [5, 6].

✉ Sankha Shuvra Das
sankha.nita.2010@gmail.com

[1] Department of Mechanical Engineering, National Institute of Technology Silchar, Silchar, Assam 788010, India

But fabrication of micro-channel on glass is a challenging issue. Various fabrication techniques have been reported by many researchers to fabricate micro-channel on glass substrates. These include wet chemical etching using different concentration of hydrofluoric acid (HF) [7, 8], micro-contact printing and wet chemical etching [9], dry etching process such as deep reactive ion etching (DRIE) using SF6 plasma [10], imprinting technique, laser micromachining, and some other processes like glass-molding process, powder blasting, ultrasonic drilling [11–16] etc.

Among all the machining process, wet chemical etching with different concentration of HF is one of the most commonly used methods for fabrication of glass micro-channel. Different etching solutions such as concentrated HF, diluted HF, HF/HCL, HF/HNO_3, HF/NH_4F/HNO_3, buffered HF (also called buffered oxide etch (BOE)) have been introduced by different researchers depending upon the composition of glass [17, 18]. But pin hole creation and lateral undercutting are the major consequences of this process. A depth of 300 μm can be achieved with SPR220-7 photoresist in combination with Cr/Au/Cr/Au metallic masking layer. The pinholes can be eliminated using this masking but lateral undercut remains a problem

[19]. Masking made of metallic layers such as Cr/Au/Ag is most popularly used masking in wet chemical etching of glass. But rapid undercutting of Cr mask during HF etching causes lateral etching than vertical etching of glass substrates after beginning of etching. This results in lesser aspect ratio of the required pattern. Moreover, it is very difficult to control the dimensions of the profile (i.e., width and depth of the channel) during etching. Various attempts have been taken by various researchers to reduce the pinhole problems in metal masking and undercutting by using multilayer of metal and thick photoresist. But the problem of undercutting still remains and etching depth more than 300 μm is found difficult to achieve. On the other hand, a high aspect ratio (more than 10), which is a very challenging issue in wet chemical etching of glass, can be obtained using DRIE process. A smooth surface finish ($R_a \sim 4$ nm) as well as a vertical etch profile (taper angle up to 88°) can be achieved, but the lower etching rate (~ 0.6 μm/min) of the process restricts its application [10].

On the other hand, laser micromachining, in this regard, offers various advantages for low thermal and mechanical damages as well as for the capability to form complex geometries. Laser machining as well as ultrasonic vibration drilling can be applied only for making thorough holes on glass substrates [16, 20]. Femtosecond laser with low pulse energy was used to fabricate micro-channel on silica glass due to their lower damage threshold [21]. A debris and crack-free laser direct-writing technology was investigated using UV laser to fabricate glass-based micro-channel. However, its long development time and circular bottom profile of the channel instead of square profile limit its scope [22]. A KrF excimer laser (λ = 248 nm) and a femtosecond laser (λ = 780 nm) were used for surface micro-machining and 3D micro-structuring on photoetchable glass ceramics. But the former process requires mask to be prepared before machining whereas later one is limited due to its low absorptivity on glass ceramics [23].

Apart from microchannel fabrication using above mentioned techniques, several non-conventional manufacturing processes were used for fabricating microstructures of various geometries. Wire cut EDM is one of the widely used methods for fabricating array of microstructures such as square micro-pillars (of 21 μm side) of higher aspect ratio (more than 33), poly-crystalline diamond micro-tools, micro end milling cutter with complex profiles etc. [24–27]. These microtools are further used for making gratings using micro end milling process.

So, from the literature, it is found that till now, numerous fabrication techniques have been introduced. But fabrication of micro-channel on glass is still a challenging issue due to the following reasons such as undercutting, difficulties in controlling the dimensions, difficulty in achieving high aspect ratio, higher surface roughness, lower absorption coefficient of glass in infrared range etc. Moreover, some of the processes are lingering, hazardous due to formation of smoke and fumes during the operation.

Therefore, looking at the limitations of the existing processes of fabrication of micro-channels on glass, a novel technique has been introduced in the present study, which will certainly contribute in the field of fabrication of micro-channel on glass substrates or any other ceramic materials. Wire-cut electro discharge machining (WEDM) and ultrasonic machining (USM) have been used to fabricate micro-channel on glass and the processes have been investigated. This technique will resolve the above mentioned problems that were encountered in various fabrication processes. Moreover, risk is eliminated as there is no use of concentrated HF or UV light in this process. No hazardous is associated with the process as there is no formation of smoke and fumes during the operation which makes the overall process eco-friendly.

2 Experimental details

Fabrication of micro-channel on glass substrate consists of two steps: (a) machining of micro-tool using WEDM and joining it with USM tool tip to make a complete tool and (b) machining of micro-channel on glass substrates using the prepared micro-tool with the help of USM.

2.1 Fabrication of micro-tool

The experiments were performed on a wire-cut electro-discharge machine (EZEE-CUT NXG). A brass wire of 250 μm diameter was used as the electrode. Dielectric fluid used for machining was prepared by mixing water with S100 coolant in the ratio of 40:1. A copper plate with dimension 100 × 60 × 1 mm was used as work piece material for micro-tool preparation in WEDM. Further, same micro-tool was used in USM for micro-channel fabrication. Copper was chosen as because it is one of the recommended materials for fabrication of USM tool.

Surface Profilometer (Handysurf E-35B) was used for measuring the surface roughness of the micro-tool. Multiple readings were taken on the vertical surfaces of the micro-tool by selecting constant gauge length, and average of these values gives the overall surface roughness of the particular tool. Optical microscope (Leica DM 2500M) was used to capture the micrographs and to measure the width of the micro-tool at various positions along its length. The average of these values was considered as the overall width of the fabricated tool.

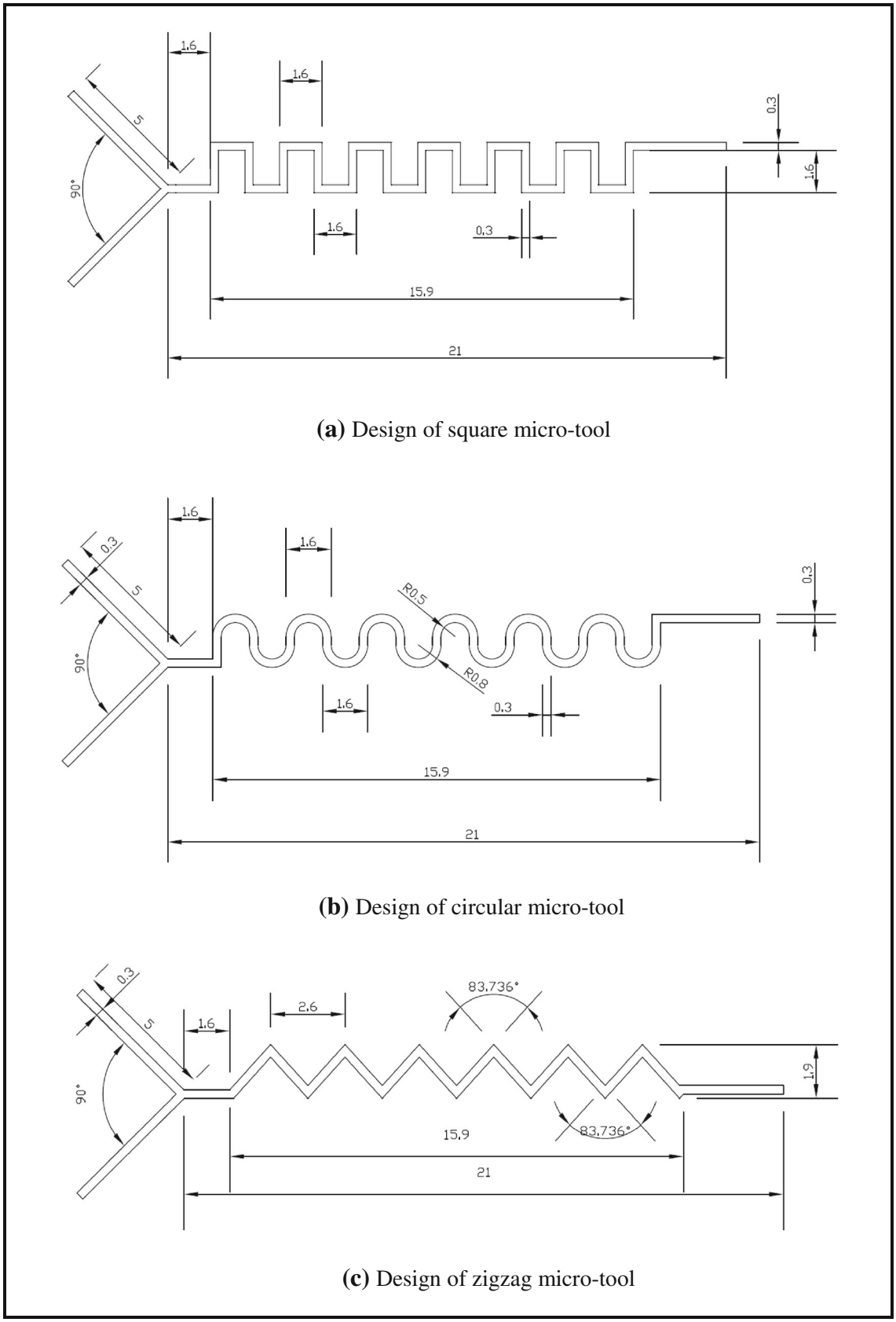

Fig. 1 **a–c** Design of micro-tools for WEDM (dimensions are in mm)

Table 1 Process parameters and their levels

Control factor	Symbols	Unit	Levels		
			I	II	III
Pulse peak current	I_p	A	1	2	3
Pulse duration	T_{on}	μs	25	32	39
Pulse off time	T_{off}	μs	6	8	10
Wire feed	W_f	mm/s	75	80	85

2.1.1 Design of micro-tool

Design of various configuration micro-tools such as square, circular, and zigzag was performed using CAD software. Figure 1 shows the design of three above mentioned configuration micro-tools. For all these configurations, width (w), pitch (P), height (H), mixing length (l), and total length (L) of the channel were 300, 2.6, 1.6, 15.9, and 21 mm, respectively. For the circular profile channel, inner and outer circle radius was 500 and 800 μm, respectively. In case of zigzag profile, the corner angle was set as 83.736°. The design information was transferred to WEDM controller for machining the micro-tool with the designed profile.

2.1.2 Selection of process parameters

In this study, four different input parameters such as peak current (I_p), pulse on time (T_{on}), pulse off time (T_{off}), wire feed rate (W_f) with three levels of each individual parameters were chosen [28]. The parameters and their levels are given in Table 1.

Taguchi method is one of the widely used techniques for finding out the optimum set of process parameters [29]. The major step towards this method is to select the process parameters accurately with their appropriate levels which may affect the output process parameters. In this study, based on the selected process parameters and their levels, Taguchi L9 array was selected for conducting the experimental runs. Each row of the orthogonal array represents a set of input parameters with which a particular experiment has to be conducted. Taguchi technique is capable of giving the trend of process parameters on the performance measures and also capable of finding out the optimized condition among the selected input parameters and their levels. The output measures selected for this experimentation were surface finish (R_a), overcut (OC), and variation in width. The input process parameters and their levels were selected after conducting pilot experiments keeping in view of output results.

2.1.3 Machining of micro-tool

Among the three above mentioned designs of micro-tools, square configuration was chosen for conducting the L9 array of experiments. For machining, brass wire (electrode) was connected to negative terminal, and copper plate (job) was connected to positive terminal of the power source. The

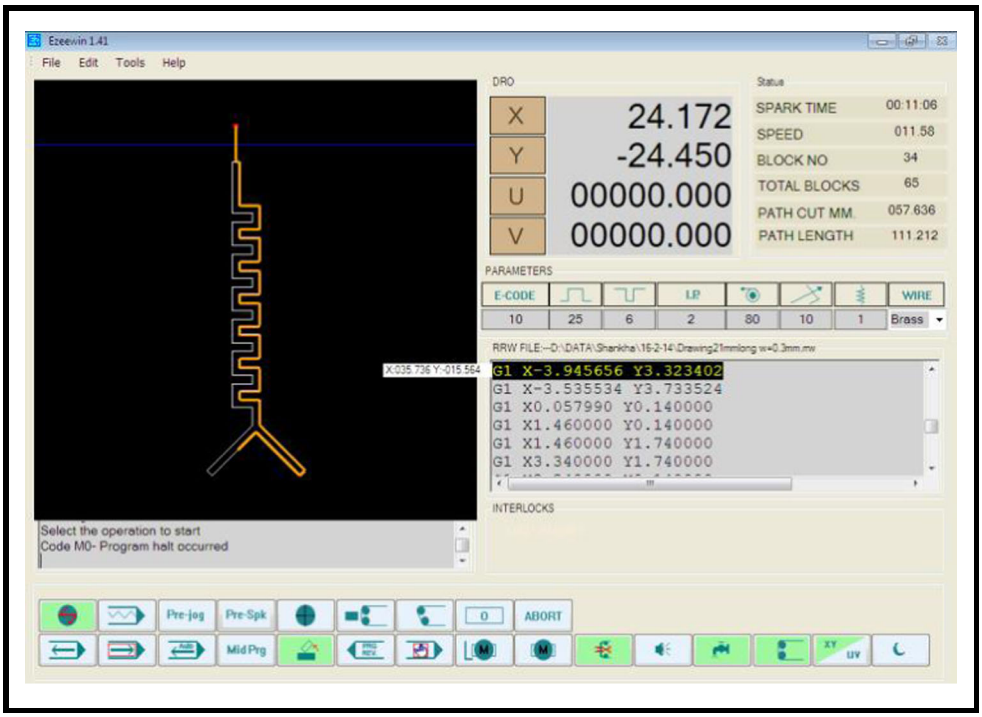

Fig. 2 WEDM console showing square profile tool

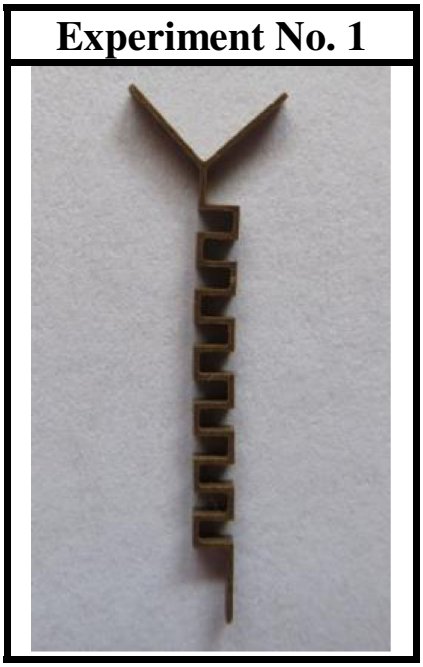

Fig. 3 WED machined square profile copper micro-tool

designed profile was fed into the WED machine controller for machining. When wire (electrode) comes in close proximity to the work piece, electric discharge occurred and hence machining takes place. The wire moves and machine following the path of the designed profile. Figure 2 shows WEDM console during machining of square profile micro-tool.

According to experimental plan, all those L9 experiments were conducted successfully for square profile tool only. The image of fabricated square profile micro-tool corresponding to first experiment of L9 array is shown in Fig. 3.

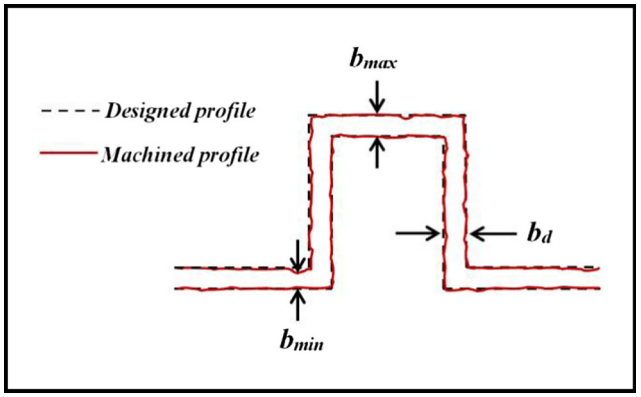

Fig. 5 Schematic of a fabricated micro-tool showing various parameters used in eqs. (1) and (2)

2.2 Parametric analysis

The purpose of this analysis was to find out a best machining condition for which overcut, surface roughness, and variation in width value will be minimum. Now to perform this, images were captured at various positions of the tool under optical microscope. Width of the micro-tool was measured at eighty one (81) different locations throughout the length which is shown in Fig. 4. The average of these values was considered as the overall or average width of the micro-tool. Same procedure was followed for measuring the average width of all nine (9) different micro-tools. Moreover, the measuring locations were identical for all the specimens. According to the design, the exact width of the micro-tool was 300 μm. The purpose of measuring overcut was to find out the amount of deviation that occurred from the exact value after machining. Any variation in the dimension of the profile was measured

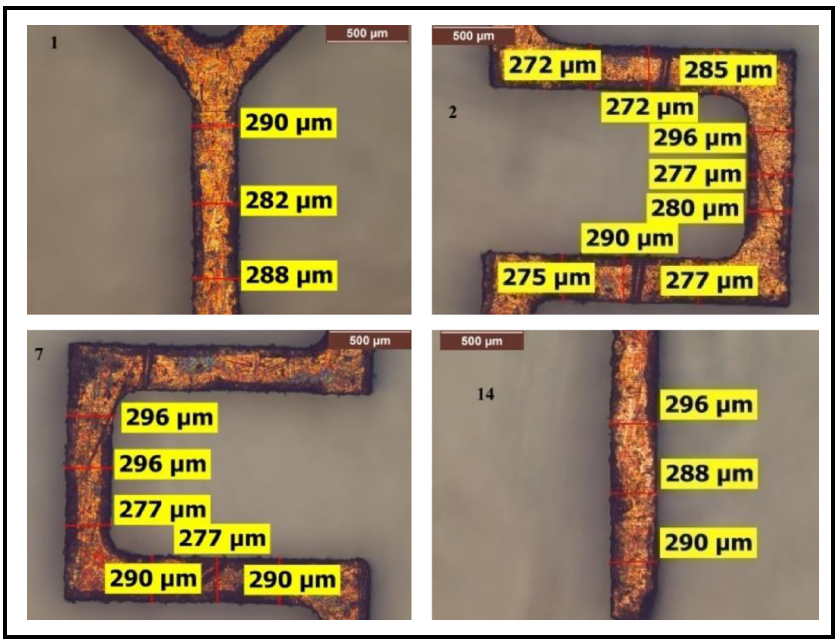

Fig. 4 Width of square profile Cu micro-tool (at different positions) measured under optical microscope

Table 2 Taguchi L9 array showing input parameters, responses, and *OEC* results (for square micro-tool)

Input parameters						Responses				
Expt. no.	T_{on} (μs)	T_{off} (μs	I_P (A)	W_f (mm/s)	Fractional overcut	Variation in width (μm)	R_a (μm) I	II	Avg. R_a (μm)	OEC
1.	25	6	1	75	0.0685	46	2.73	2.86	2.795	98.76
2.	25	8	2	80	0.1321	69	3.37	3.86	3.615	47.84
3.	25	10	3	85	0.1554	87	4.11	4.30	4.205	16.96
4.	32	6	2	85	0.117	49	3.86	4.20	4.030	61.72
5.	32	8	3	75	0.1729	63	5.3	4.46	4.880	19.83
6.	32	10	1	80	0.0645	75	2.82	2.79	2.805	76.82
7.	39	6	3	80	0.158	88	4.2	5.3	4.750	6.66
8.	39	8	1	85	0.1021	58	3.11	3.34	3.225	72.03
9.	39	10	2	75	0.1254	63	3.8	5.49	4.645	38.2

from this value only. The thickness of the micro-tool obtained after WEDM is 1 mm. In micro-channel, wall roughness is a critical factor. As the tool shape would be replicated in the channel while ultrasonic machining, surface roughness of the tool should be minimum to get a micro-channel with less rougher wall. On the other hand, variation in width of the tool will give the idea regarding the uniformity of width throughout the channel. After machining, it was found that at some position, the width of the profile became narrow, and in some other location, it was wider. This may be the consequence of using a re-circulating brass wire for machining instead of single pass wire. Thus, the wire gets spark eroded and became thin as well as non-uniform as the number of times wire passes through the machining site. Now, during machining, the profile would be uniform till the fresh side of the wire appears to the job. Further, the profile would be non-uniform upon machining by the already eroded wire surface. So, the variation in width was nothing but the difference between the maximum and the minimum value of width throughout the tool profile. The value of overcut and variation in width was calculated using eqs. (1) and (2).

$$\textit{Fractional over cut},\quad OC = \frac{b_d - b_a}{b_d} \tag{1}$$

Table 3 Analysis of variance (ANOVA)

(a) for 100% R_a					
Factor	DOF (f)	Sum of squares (S)	Variance (V)	Pure sum (S′)	Percent P (%)
T_{on}	2	0.672	0.336	0.672	12.675
T_{off}	2	0.003	0.001	0.003	0.066
I_p	2	4.388	2.194	4.388	82.758
W_f	2	0.238	0.119	0.238	4.497
Other/error	0	–	–	–	–
Total	8	5.302			100%
(b) for 100% overcut					
T_{on}	2	0	0	0	1.816
T_{off}	2	0	0	0	7.36
I_p	2	0.01	0.005	0.01	89.408
W_f	2	0	0	0	0.567
Other/error	0	–	–	–	–
Total	8	0.011			100%
(c) for 100% variation in width					
T_{on}	2	84.221	42.11	84.221	4.72
T_{off}	2	337.555	168.777	337.555	18.918
I_p	2	748.223	374.111	748.223	41.935
W_f	2	614.221	307.11	614.221	34.425
Other/error	0	–	–	–	–
Total	8	1784.222			100%
(d) for OEC					
T_{on}	2	436.178	218.089	436.178	5.642
T_{off}	2	227.642	113.821	227.642	2.945
I_p	2	6947.988	3473.994	6947.988	89.886
W_f	2	117.962	58.981	117.962	1.526
Other/error	0	–	–	–	–
Total	8	7729.773			100%

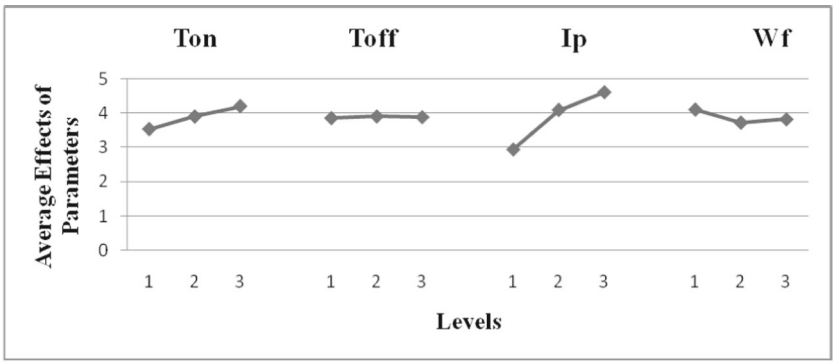

(a)

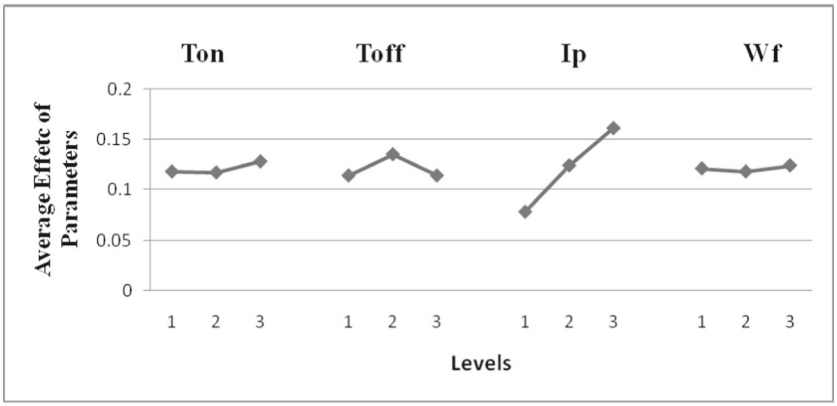

(b)

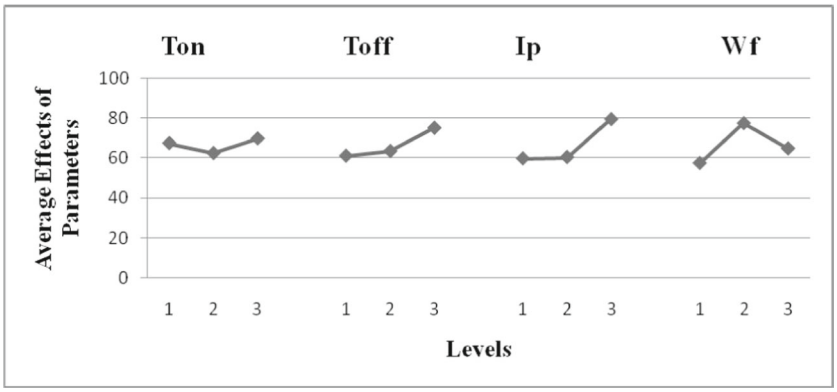

(c)

Fig. 6 Average effect of parameters and their level at **a** 100% R_a, **b** 100% OC, **c** 100% variation in width

$$Variation\ in\ width = b_{max} - b_{min} \quad (2)$$

where b_d = designed width of micro-tool, b_a = average width of micro-tool achieved, b_{max} = maximum width of the micro-tool, b_{min} = minimum width of the micro-tool.

Figure 5 shows different parameters used to calculate fractional overcut and variation in width in eqs. (1) and (2), respectively. Here, fractional overcut is considered to reduce error only. However, one may consider overcut for the analysis, and in that case, eq. (1) will change. Analysis of variance (ANOVA) of the experimental data was performed to obtain the percentage contribution of the factors and their significance. Individual analysis was performed considering 100% R_a, 100% overcut, and 100% variation in width.

To obtain multiple objectives, a single index named overall evaluation criteria (*OEC*) was performed. It was performed by combining three performance measures. The formulation for calculating *OEC* for two output measures *X* and *Y* with weightage of *Wx* and *Wy* is shown in eq. (3). The relative weightage is subjective and assigned to each individual criterion as per its preference and its effect desirable in the results [29]. Where quality characteristics (*QC*) for X is larger-is-the-best (*QC* = *L*) and for Y is smaller-is-the-best (*QC* = *S*).

Table 4 Optimum condition and performance

(a) at 100% R_a			
Factor	Level description	Level	Contribution
T_{on}	25	1	− 0.346
T_{off}	6	1	− 0.025
I_p	1	1	− 0.942
W_f	80	2	− 0.161
Total contribution from all factors			− 1. 474
Current grand average of performance			3.883
Expected result at optimum condition			*2.409*
(b) at 100% OC			
T_{on}	32	2	− 0.004
T_{off}	6	1	− 0.008
I_p	1	1	− 0.044
W_f	80	2	− 0.004
Total contribution from all factors			− 0.06
Current grand average of performance			0.121
Expected result at optimum condition			*0.061*
(c) at 100% variation in width			
T_{on}	32	2	− 4.112
T_{off}	6	1	− 5.445
I_p	1	1	− 6.778
W_f	75	1	− 9.112
Total contribution from all factors			− 25.447
Current grand average of performance			66.444
Expected result at optimum condition			*40.997*
(d) for OEC			
T_{on}	25	1	5.762
T_{off}	6	1	6.955
I_p	1	1	33.778
W_f	75	1	3.505
Total contribution from all factors			50
Current grand average of performance			48.757
Expected result at optimum condition			**98.757**

Table 5 Optimum condition for R_a, OC, and variation in width

Sl. No.	Factor (s)	Optimum condition for response(s)			
		R_a	OC	Variation in width	OEC
1	T_{on}	25 (μs)	32 (μs)	32 (μs)	25 (μs)
2	T_{off}	6 (μs)	6 (μs)	6 (μs)	6 (μs)
3	I_p	1 (A)	1 (A)	1(A)	1 (A)
4	W_f	80 (mm/s)	80 (mm/s)	75 (mm/s)	75 (mm/s)

$$OEC = \frac{X - X\min}{X\max - X\min} \times Wx + \left(1 - \frac{Y - Y\min}{Y\max - X\min}\right) \times Wy \quad (3)$$

Initially, ANOVA was performed giving 100% weightage to each individual output parameters followed by three confirmation experiments. Then, to give equal weightage to all the output process parameters, *OEC* was performed by giving 33.33% weightage to R_a, 33.34% weightage to overcut, and 33.33% weightage to variation in width. The analysis of *OEC* results was performed by taking, "Larger is the Best" in order to maximize OEC. Table 2 shows Taguchi L9 orthogonal array with input process parameters, output parameters or responses, and *OEC* results.

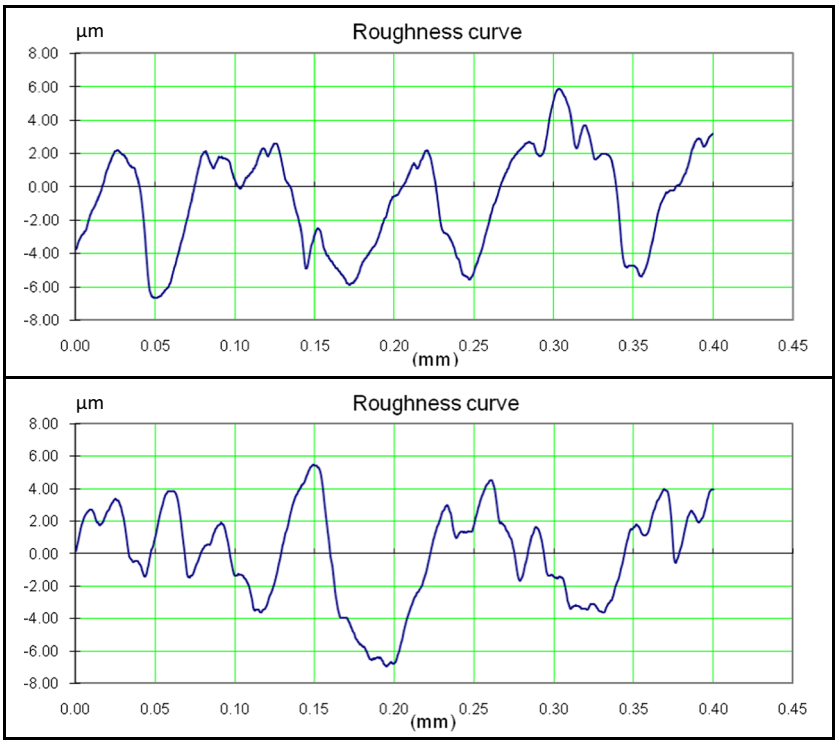

Fig. 7 Surface profile curve of confirmation test (for square profile)

Table 6 OEC for 33.33% Ra, 33.34% overcut, and 33.33% variation in width

Sl. No.	Responses	Worst value	Best value	QC	Relative weightage
1.	R_a (μm)	4.88	2.795	S	33.33
2.	Fractional overcut	0.1729	0.0645	S	33.34
3.	Variation in width (μm)	88	46	S	33.33

2.2.1 Analysis for surface roughness

For each sample, surface roughness was measured at two different locations R_a (I) and R_a (II) and the corresponding values are given in Table 2. ANOVA was performed by giving 100% weightage to average surface roughness (R_a) of R_a (I) and R_a (II), and the result of analysis is shown in Table 3(a). It was observed that peak current, I_p, has the most significant effect with a contribution of 82.758%. However, T_{on} has moderate effect with a contribution of 12.675% on R_a. On the other hand, W_f and T_{off} have least effect with a contribution of 4.497 and 0.066% on surface roughness, respectively. The parameters whose contribution is less than 10% considered as insignificant parameter [30]. The average effect of different process parameters with respect to their levels for R_a is shown in Fig. 6a. It shows that with increase in T_{on} and I_p, R_a also increases which may be due to high heat generation at the cutting zone that causes larger crater formation resulting in higher R_a. On the other hand, as W_f increases, R_a decreases which may be due to appearing the new side of the wire quickly at the cutting site. The optimum condition achieved for minimum R_a was $T_{on} = 25$ μs, $T_{off} = 6$ μs, $I_p = 1$A, and $W_f = 80$ mm/s that is represented in Table 4(a). Further, this optimum condition was used for conducting the confirmation experiment. After confirmation experiment, the average R_a value was obtained as 2.55 μm while the expected R_a value at optimum condition after ANOVA was 2.409 μm which was quite comparable. The surface profile (roughness) curve of the confirmation experiment is shown in Fig. 7.

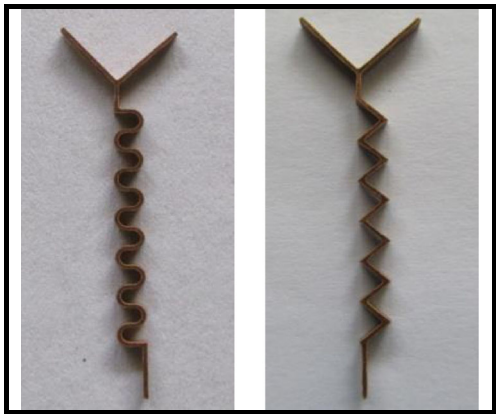

Fig. 9 Photographs of circular (left) and zigzag (right) profile WED machined Cu micro-tool

2.2.2 Analysis for overcut

By giving 100% weightage to overcut (OC) value, ANOVA was performed and the result is shown in Table 3(b). Here, peak current, I_p, was the most effective parameter with a significant contribution of 89.408% on overcut. On the other hand, T_{off} and T_{on} have only 7.36 and 1.816% contribution, respectively. W_f has almost no effect on overcut. Figure 6b shows the average effect of process parameters on overcut with respect to their three different levels. As I_p increases, heat generation at the cutting zone increases which causes larger material removal at the cutting zone resulting in more chances of overcut. As T_{off} increases, initially overcut increases, but finally, it decreases which may be due to formation of recast layer at the cutting zone. From Table 4(b), it was found that the optimum condition for obtaining minimum OC was $T_{on} = 32$ μs, $T_{off} = 6$ μs, $I_p = 1$ A, and $W_f = 80$ mm/s. The value of overcut after confirmation experiment was obtained as 0.060 whereas the expected overcut value after ANOVA was obtained as 0.061 which was again quite comparable.

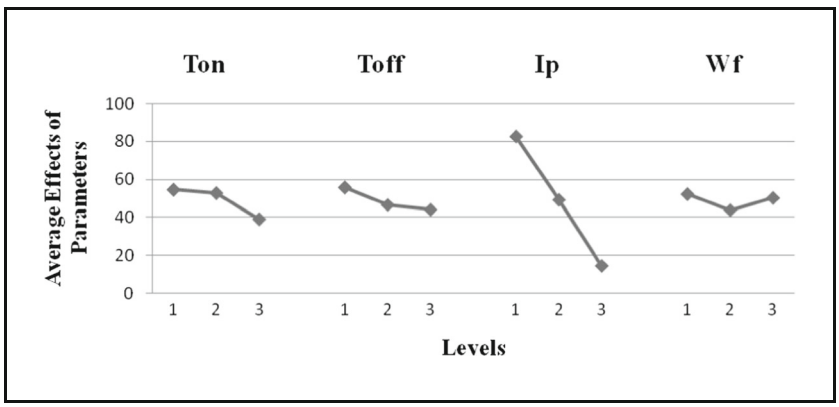

Fig. 8 Average effect of parameters with respect to their level of OEC

Table 7 Various input process parameters and responses for circular and zigzag profile micro-tool

Input parameters					Responses				
Tool type	T_{on} (μs)	T_{off} (μs	I_P (A)	W_f (mm/s)	Fractional overcut	Variation in width (μm)	R_a (μm) I	II	Avg. R_a (μm)
Circular	25	6	1	75	0.041	48	2.96	2.46	2.71
Zigzag	25	6	1	75	0.037	41	2.93	2.42	2.675

2.2.3 Analysis for variation in width

ANOVA was performed by considering 100% weightage to the variation in width and the result is shown in Table 3(c).

From ANOVA, I_p and W_f were identified as the most significant parameter with a contribution of 41.935 and 34.425%, respectively. However, T_{off} has the moderate effect with a contribution of 18.918%. T_{on} was found as insignificant parameter as its contribution was 4.72% only. Figure 6c shows the average effect of parameters on variation in width with respect to their different levels. Similar to former cases, here also variation in width increases with increase in I_p and the reason is identical as earlier. For increase in T_{on}, variation in width initially decreases but later on increases. This may be due to higher electrical energy delivered for a longer time causes larger work material removal as well as tool (wire) wear. Now, as the same wire is circulating again and again, it will wear out in every pass and ultimately causes dimensional error after each pass. So, the part which will be machined with fresh wire will give minimum deviation than the part which will be machined by the worn out wire. Therefore, as T_{on} increases, the wire will wear out more rapidly that causes increase in variation in width. As wire feed rate increases, initially variation in width increases and finally deceases and that may be due to the similar reason as explained in the earlier sections. The optimum condition for minimum variation in width was $T_{on} = 32$ μs, $T_{off} = 6$ μs, $I_p = 1$ A, and $W_f = 75$ mm/s which is demonstrated in Table 4(c). The value of variation in width after confirmation experiment was obtained as 46 μm while the expected value after ANOVA was found as 40.997 μm which was relatively comparable. The optimum condition for all the responses is given in Table 5.

2.2.4 OEC analysis

OEC was performed by considering 33.33% weightage to R_a, 33.34% weightage to overcut, and 33.33% weightage to variation in width. In all these cases, quality characteristics (QC) is considered as "smaller is the best (S)" which is shown in the Table 6. The calculated values of OEC for Taguchi L9 experiments are shown in Table 2. ANOVA was performed for OEC values, and the percentage contribution of the individual parameters is shown in Table 3(d). The peak current, I_p, was the most influential factor as it contributes 89.886% on OEC. On the other hand, T_{off}, T_{on}, and W_f had insignificant effect with contribution of 5.642, 2.945, and 1.526%, respectively. Table 4(d) represents the optimum condition for OEC as $T_{on} = 25$ μs, $T_{off} = 6$ μs, $I_p = 1$ A, and $W_f = 75$ mm/s which matches with the experiment no. 1 of L9 array. The OEC value for experiment 1 was obtained as 98.76 whereas the expected result at optimum condition was achieved as 98.757 and both were quite comparable. Therefore, this would be selected as optimum set of parameters out of all the experiments and will be used for further machining. Hence, it was not required to conduct any further confirmation experiment. The average effect of process parameters on OEC with respect to their different levels is shown in Fig. 8.

The optimum set of parameters which were found after OEC, used for further machining of circular and zigzag profile micro-tools. Figure 9 shows the photographs of circular and zigzag profile micro-tool. The width of the circular and zigzag tool was also measured under optical microscope by considering the same procedure that followed for square tool. The input and output parameter values of circular and zigzag profile micro-tool are listed in Table 7.

Fig. 10 Different soft soldered USM micro-tool assemblies (from left to right: square, circular, and zigzag)

Table 8 Input parameters for machining serpentine micro-channel on glass using USM

Type of micro-channel	Power rating (%)	Current (mA)	Feed rate (mm/s)	Abrasive		Feed force (kg)	Machining time[a]
	Range (20–100)	Range (0–100)	For glass (0.025–0.125)	Type	Grit		
Square profile	40	12	0.0625	B_4C	400	0.9	49 s
	50	13	0.0625				43 s
	60	14	0.0625				36 s
Circular profile	40	12	0.0625				74 s
	50	13	0.0625				56 s
	60	14	0.0625				42 s
Zigzag profile	40	12	0.0625	B_4C	400	0.9	54 s
	50	13	0.0625				42 s
	60	14	0.0625				33 s

[a] After deduction of idle time

After WED machining, the average width of micro-tools obtained as 279.43, 287.82, and 288.90 μm for square, circular, and zigzag profile micro-tool, respectively. Hence, the deviation of actual dimension (i.e., average width) from designed dimension (i.e., exact width) of the fabricated micro-tool is 20.57, 12.18, and 11.1 μm for square, circular, and zigzag profile geometry, respectively.

2.3 Joining of micro-tool with USM tool tip

It was recommended to maintain the weight of the Cu micro-tool less than or equal to 1 gm for the existing USM setup, otherwise proper tuning may not be achieved. Precision Analytical Balance (Ishida DXR-220) was used for measuring the weight of the micro-tool after machining. The weight of the square, circular, and zigzag micro-tool was obtained as 0.1861, 0.1640, and 0.1610 gm, respectively, which were within the stated range. The weight of USM tool tip was measured as 41.9631 gm. Soft silver soldering was performed for joining Cu micro-tool with tool tip of USM at a temperature of 350–450 °C. The micro-tool assemblies after soldering are shown in Fig. 10. Further, these tool assemblies were connected to the horn of the USM using mechanical threading process and used for machining micro-channels.

2.4 Fabrication of serpentine micro-channels using USM

All the experiments were performed on "AP-1000" (SONICMILL) with 1000-W output power ultrasonic machine. The power rating of this machine varies from 20 to 100% whereas tuning current varies from 0 to 100 mA. The entire experimental setup of USM consists of power source, control unit (Autopac IIb), slurry delivery system, and mill module. The power supply unit of the device converts 50 Hz electrical signal to 20 kHz electrical signal. A piezoelectric transducer is used to transform this high-frequency electrical signal to high-frequency mechanical vibration. Thus, the frequency of vibration of this machine was set to 20 kHz (as per machine manual). A coupler is used to transfer the high-frequency vibration to horn of the machine. A coupler may have different configurations according to amplitude requirement for

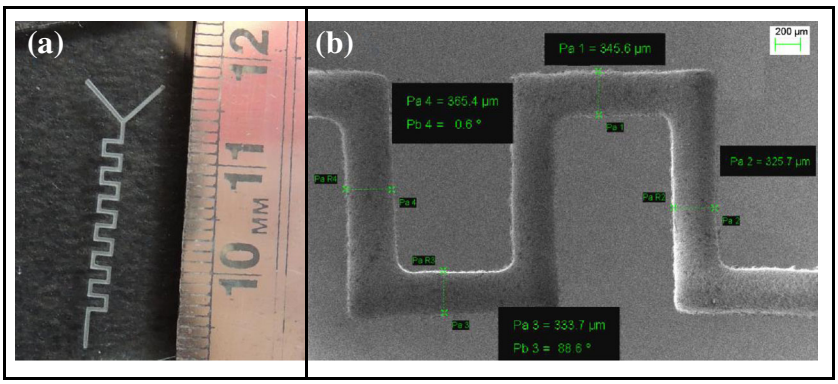

Fig. 11 **a** Square profile serpentine micro-channel fabricated (in 40% power rating) on glass. **b** FESEM image of the channel

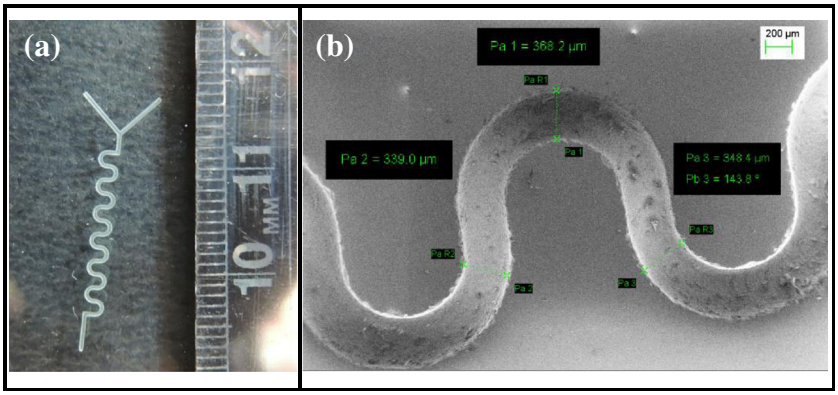

Fig. 12 **a** Circular profile serpentine micro-channel fabricated (in 40% power rating) on glass. **b** FESEM image of the channel

machining. In this experiment, a green coupler (1:1) was used. The shape of the horn is such that it concentrates and amplifies the vibration in a very small area and transmits it to the tool tip. As the tool tip vibrates, abrasive particle indents the work surface resulting in crack initiation at the indentation site. With further loading, crack propagates and ultimately brittle fracture of the material takes place. The debris particle from the machining zone is flushed away by a jet of abrasive slurry during the backward stroke of the horn.

2.4.1 Selection of process parameters

The input parameters used for fabrication of square, circular, and zigzag configuration serpentine micro-channel on glass are represented in Table 8. In this study, power supply rate of 40–60% at 1000 W power range has been selected. Feed rate was chosen as 0.0625 mm/s that were in the recommended range of feed rate (0.025–0.125 mm/s) for glass. The abrasive slurry was prepared by mixing boron carbide powder of 400 grit size (~23 μm grit diameter) with water in 1:1 ratio (slurry concentration ~ 50%). Further, the slurry flow was kept constant at 6 l/min for all the experiments [31]. Feed force was selected as 0.9 kg which was constant throughout the process. For 20-kHz vibration frequency, the amplitude of tool vibration was approximately 30–40 μm for all the experiments (as per machine manual). A glass specimen with 70 × 50 × 4 mm size was used as work piece material.

2.4.2 Machining of square, circular, and zigzag profile micro-channels

Serpentine micro-channels of square, circular, and zigzag profiles were fabricated with different power rating such as 40, 50, and 60%. During machining, corresponding machining time required for fabrication of individual micro-channel was measured. The machining time was not much point of concern, but still, it gives an idea regarding the productivity of this novel technique. After experimentation, it was found that machining time required for fabrication of each square profile micro-channel was almost equal or less than one (1) minute in almost all power ratings. Here, machining time decreases as power rating increases. In USM, power rating is one of the main machining parameters in regard to the energy of USM. However, current in Table 8 is the tuning current with respect to the different power rating which is recorded during the experiment. Here, it is found that as power rating increases, machining time decreases or the material removal rate increases. As power rating increases, the abrasive particles

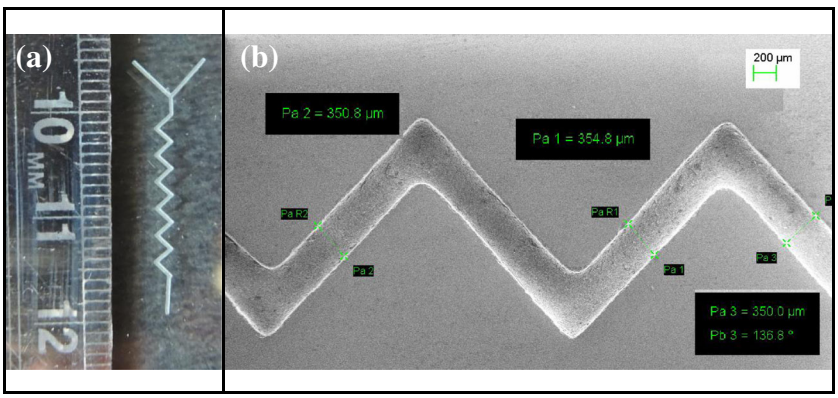

Fig. 13 **a** Zigzag profile serpentine micro-channel fabricated (in 40% power rating) on glass. **b** FESEM image of the channel

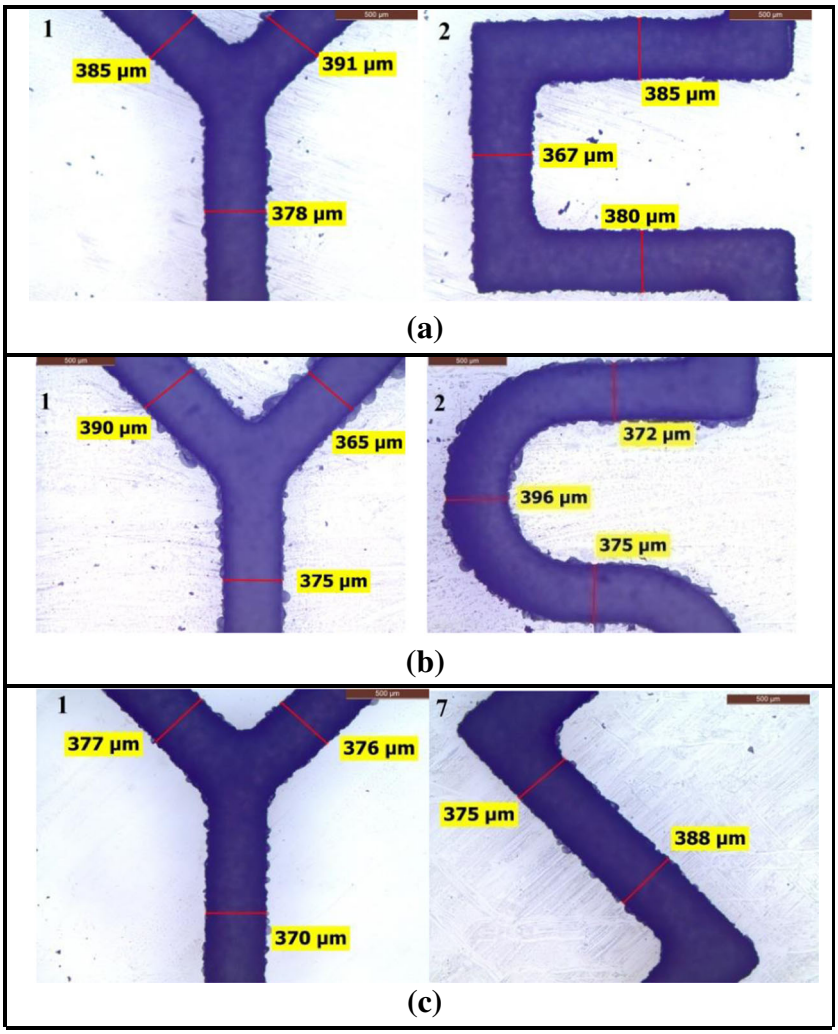

Fig. 14 Microscopic images of **a** square profile, **b** circular profile, and **c** zigzag profile glass serpentine micro-channel

strike the work surface with more momentum as well as more kinetic energy. This results in larger crater formation and hence higher material removal rate [32]. Figure 11a, b shows the digital and field emission scanning electron microscopy (FESEM) image the square profile serpentine micro-channel (after machining). Similarly, machining time noted for fabrication of individual circular profile micro-channel was less than one (1) minute. During machining of zigzag profile micro-channel, time recorded for the fabrication of single micro-channels was 54, 42, and 33 s in 40, 50, and 60% power rating, respectively. Table 8 shows the machining time required for fabrication of various configuration micro-channels with different power ratings.

The digital and FESEM images of circular and zigzag profile micro-channel after machining are represented in Figs. 12a, b and 13a, b, respectively. The width of the micro-channels was measured under optical microscope, and the photographs of all the channels are displayed in Fig. 14.

The width was measured at twenty-nine (29) different locations throughout the channel length, and finally, average width was considered for all the micro-channels and values are given in Table 9. The average width of square, circular,

Table 9 Dimensions of square, circular, and zigzag profile glass micro-channels after US machining

Type of channel	Width of micro-channel (avg.) (μm)	Width of micro-tool (avg.) (μm)	Gross overcut (μm)	Net overcut (μm)	Depth of micro-channel (μm)
Square	374.65	279.43	95.22	74.65	165–170 μm
Circular	375.86	287.82	88.04	75.86	
Zigzag	381.75	288.90	92.85	81.75	

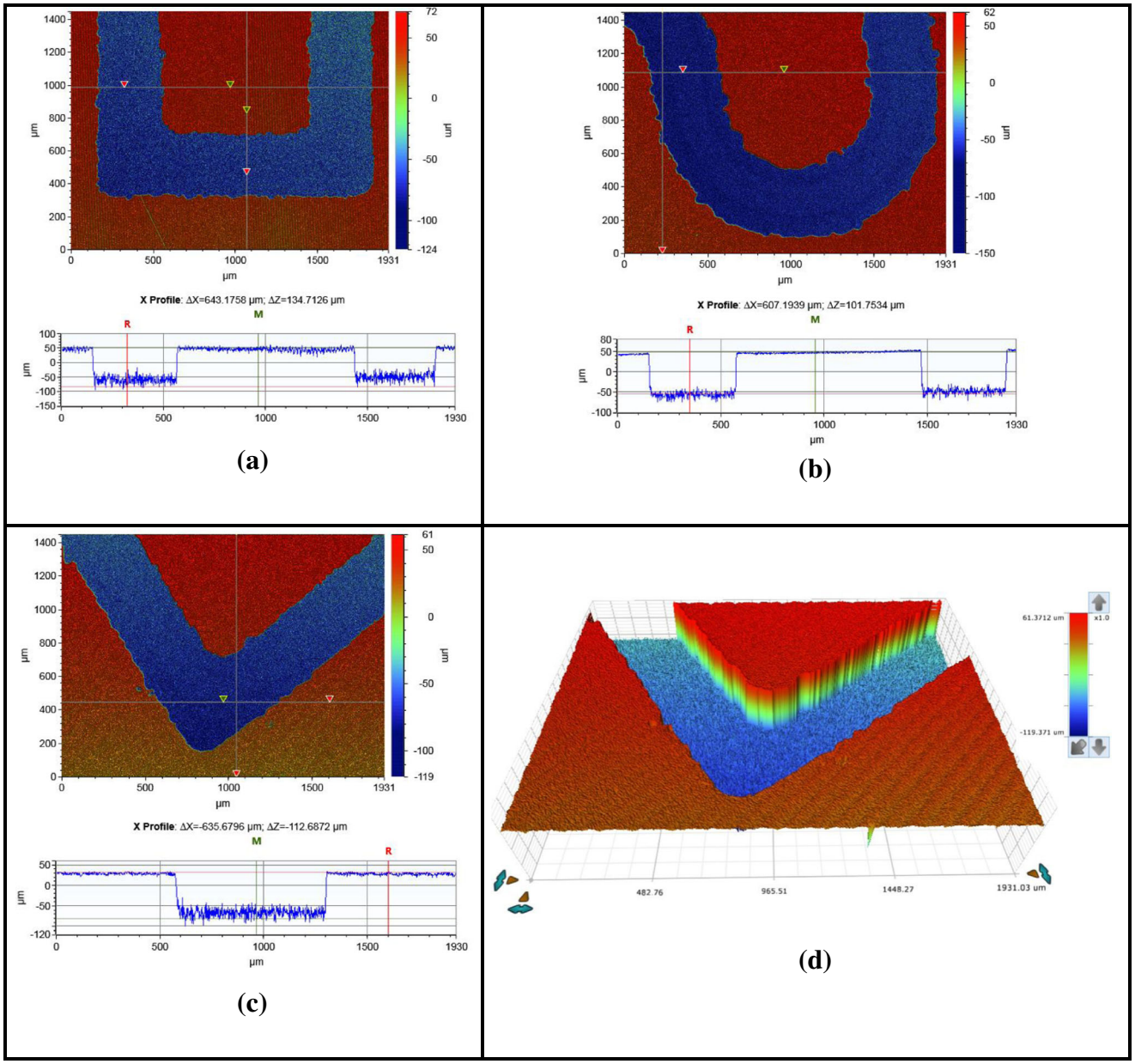

Fig. 15 Measured depth of **a** 2D square profile, **b** 2D circular profile, **c** 2D zigzag profile, and **d** 3D zigzag profile serpentine micro-channel

and zigzag profile micro-channels obtained as 374.65, 375.86, and 381.75 µm, respectively. The channel width after machining became more than the width of the micro-tool. Thus, gross overcut became 95.22 µm for square profile micro-tool which was calculated using eq. (4).

This overcut is absolutely dependent on grit size of the abrasives, and it can be smaller if finer grit is used. As the designed width of micro-tool was 300 µm, the net overcut of the micro-channel obtained after machining as 74.65 µm which was calculated using eq. (5). Similarly, gross overcut and net overcut found for circular micro-channels were 88.04 and 75.86 µm, respectively. For zigzag micro-channels also, gross overcut and net overcut obtained as 92.85 and 81.75 µm, respectively.

$$\textit{Gross Over cut} = b_c - b_a \tag{4}$$

$$\text{Net } \textit{Over cut} = b_c - b_d \tag{5}$$

$$\textit{Depth Variation} = d_m - d_a \tag{6}$$

where b_c = average width of micro-channel achieved, b_a = average width of micro-tool achieved, b_d = designed width of micro-tool, d_m = set value of depth before USM (z-movement of the tool), d_a = depth of the micro-channel achieved after USM.

3D non-contact optical surface profilometer (BRUKER, Contour GT) was used to measure the depth of micro-

channels. The depth was measured (only X profile) at various locations along the track and found as ~ 135, ~ 102, and ~ 113 μm for square, circular, and zigzag profile channel, respectively. The 2D and 3D profile of the fabricated channels is shown in Fig. 15.

3 Discussions

The accuracy in terms of width of the micro-channels depends on the accuracy of the Cu micro-tool fabricated using WEDM. The variation in width, i.e., uniformity of the micro-tool and surface roughness of the micro-tool which will be reflected into the micro-channel wall were considered as an important parameter in this study.

The net overcut in the micro-channel depends on several factors such as the diameter of the electrode wire used in WEDM and the spark gap. As wire diameter increases, overcut increases with it. The spark gap increases with the increase in gap voltage and which in turn increases fractional overcut in WEDM. The abrasive particle size has also the influence on overcut in USM. As the particle size increases, overcut also increases. Overcut is an unavoidable phenomenon because of the inherent characteristics of the used manufacturing processes, WEDM and USM. But it can be controlled with proper selection of process parameters. The net overcut can be compensated by calibrating the size of the tool considering the value of the overcut during the fabrication of micro-tool.

In this process, under cut (i.e., machining below the masking) is not relevant because masking is not used at all in this technique. The channel dimensions fabricated using this process found to have good accuracy. The required depth can be obtained by pre-setting it before machining without any difficulty. Hence, higher aspect ratio can easily be obtained in this process. The process is very simple, less time consuming, and productive as it takes only a few seconds to fabricate a micro-channel in difficult to machine materials like glass, ceramics etc.

4 Conclusions

Serpentine micro-channels of different configurations such as square, circular, and zigzag profile were fabricated successfully on glass substrates using a novel technique that uses wire-cut electro discharge machining and ultrasonic machining. Taguchi design of experiments was performed for conducting the experiments, and finally, ANOVA and OEC were done to find out the optimum set of parameters. Initially, square profile Cu micro-tool was fabricated using Taguchi L9 orthogonal array and optimum condition of process parameters was obtained as T_{on} is 25 μs, T_{off} is 6 μs, I_p is 1 A, and W_f is 75 mm/s. The fractional overcut, variation in width, and surface roughness obtained as 0.0685, 46, and 2.795 μm, respectively, at the optimum condition. Finally, ultrasonic machining was performed for fabrication of serpentine micro-channels of different configurations using the fabricated micro-tools. The net overcut found as 74.65, 75.86, and 81.75 μm for square, circular, and zigzag profile micro-channels, respectively. The depth was obtained as ~ 135, ~ 102, and ~ 113 μm for square, circular, and zigzag profile micro-channel, respectively. Thus, this method can be used for fabricating microchannel of different geometries on glass substrate or any ceramic surface. Further, these fabricated channels can be exploited for any microfluidic application such as micro-mixing, cell sorting, DNA sequencing, medical diagnostics, droplet generation etc. Moreover, the fabrication method is very fast and hence the process is productive and less hazardous.

References

1. Ali MY (2009) Fabrication of micro-fluidic channel using micro end milling and micro electrical discharge milling. Int J Mech Mater Eng 4:93–97
2. Yu H, Zhou G, Chau FS, Wang S, Lee F (2009) Novel polydimethylsiloxane (PDMS) based micro-channel fabrication method for lab-on-a-chip application. Sensors Actuators B Chem 137:754–761
3. Nikumb S, Chen Q, Li C, Reshel H, Zheng HY, Qiu H, Low D (2005) Precision glass machining, drilling and profile cutting by short pulse lasers. Thin Solid Films 477(1-2):216–221. https://doi.org/10.1016/j.tsf.2004.08.136
4. Cheng Y, Sugioka K, Midorikawa K (2004) Microfluidic laser embedded in glass by three-dimensional femtosecond laser microprocessing. Opt Lett 29(17):2007–2009. https://doi.org/10.1364/OL.29.002007
5. Huang CY, Kuo CH, Hsiao WT, Huang KC, Tseng SF, Chou CP (2012) Glass biochip fabrication by laser micromachining and glass-molding process. J Mater Process Technol 212(3):633–639. https://doi.org/10.1016/j.jmatprotec.2011.10.013
6. Edouard T, Florian D, Edmond C, Charlie G (2006) Reactive ion etching of glass for biochip applications: composition effects and surface damages. Microelectron Eng 83:1155–1158
7. Spiering GACM (1993) Review-wet chemical etching of silicate glasses in hydrofluoric acid based solutions. Mater Sci 28(23):6261–6273. https://doi.org/10.1007/BF01352182
8. Iliescu C, Tay FEH, Miao J (2007) Strategies in deep wet etching of Pyrex glass. Sensors Actuators A133:395–400
9. Hannes B, Vieillard J, Chakra EB et al (2008) The etching of glass patterned by micro-contact printing with application to microfluidics and electrophoresis. Sensors Actuators B Chem 129(1):255–262. https://doi.org/10.1016/j.snb.2007.08.025
10. Li XD, Abe T, Esashi M (2008) Deep reactive ion etching of Pyrex glass using SF6 plasma. Sens Actuators A 87:139–145
11. Chen Q, Chen Q, Maccioni G (2013) Fabrication of micro-fluidics structures on different glasses by simplified imprinting technique. Curr Appl Phys 13(1):256–261. https://doi.org/10.1016/j.cap.2012.07.019
12. Tseng SF, Chen MF, Hsiao WT, Huang CY, Yang CH, Chen YS (2014) Laser micro-milling of convex micro-fluidic channels onto glassy carbon for glass molding dies. Opt Lasers Eng 57:58–63. https://doi.org/10.1016/j.optlaseng.2013.11.011

13. Huang CY, Kuo CH, Hsiao WT, Huang KC, Tseng SF, Chou CP (2012) Glass biochip fabrication by laser micro-machining and glass-molding process. J Mater Process Technol 212(3):633–639. https://doi.org/10.1016/j.jmatprotec.2011.10.013
14. Issa A, Brabazon D, Hashmi MSJ (2008) 3D transient thermal modelling of laser micro-channel fabrication in lime-soda glass. J Mater Process Technol 207(1-3):307–314. https://doi.org/10.1016/j.jmatprotec.2008.06.056
15. Belloy E, Sayah A, Gijs MAM (2000) Powder blasting for three-dimensional micro-structuring of glass. Sens Actuators 86(3):231–237. https://doi.org/10.1016/S0924-4247(00)00447-7
16. Voisey KT (2014) Laser drilling of metallic and non-metallic materials and quality Assesment. Compr Mater Process Laser Mach Surf Treat 9:177–194
17. Iliescu C, Jing J, Tay FEH, Miao J, Sun T (2005) Characterization of masking layers for deep wet etching of glass in an improved HF/HCl solution. Surf Coat Technol 198(1-3):314–318. https://doi.org/10.1016/j.surfcoat.2004.10.094
18. He Q, Chen S, Su Y, Qun F, Chen H (2008) Fabrication of 1D nano-fluidic channels on glass substrate by wet etching and room-temperature bonding. Anal Chim Acta 628(1):1–8. https://doi.org/10.1016/j.aca.2008.08.040
19. Bu M, Melvin T, Ensell GJ, Wilkinson JS, Evans AGR (2004) A new masking Technology for Deep Glass Etching and its micro-fluidic application. Sens Actuators A 115(2-3):476–482. https://doi.org/10.1016/j.sna.2003.12.013
20. Egashira K, Mizutani K, Nagao T (2002) Ultrasonic vibration Drilling of Micro-Holes in glass. CIRP Ann Manuf Technol 51(1):339–342. https://doi.org/10.1016/S0007-8506(07)61531-5
21. Quan S, Ali S, Francis T, Real V, See LC (2008) Micro-channel fabrication in silica glass by femtosecond laser pulses with different central wavelengths. J Micromech Microeng 18:35–39
22. Cheng J-Y, Yen M-H, Wei C-W, Chuang Y-C, Young T-H (2005) Crack-free direct-writing on glass using a low-power UV laser in the manufacture of a micro-fluidic chip. J Micromech Microeng 15(6):1147–1156. https://doi.org/10.1088/0960-1317/15/6/005
23. Joohan K, Halil B, Xianfan X (2004) Fabrication of microstructures in photoetchable glass ceramics using excimer and femtosecond lasers. J Microlith Microfab Microsyst 3:478–485
24. Fonda P, Katahira K, Kobayashi Y, Yamazaki K (2012) WEDM condition parameter optimization for PCD microtool geometry fabrication process and quality improvement. Int J Adv Manuf Technol 63(9-12):1011–1019. https://doi.org/10.1007/s00170-012-3977-7
25. Zhong L, Liang L, Wu X, He N, Zhao G, Yao C (2017) Fabrication of PCD micro cutting tool and experimental investigation on machining of copper grating. Int J Adv Manuf Technol 88(9-12):2417–2427. https://doi.org/10.1007/s00170-016-8793-z
26. Yan J, Uchida K, Yoshihara N, Kuriyagawa T (2009) Fabrication of micro end mills by wire EDM and some micro cutting tests. J Micromech Microeng 19(2):025004 **(1-9)**. https://doi.org/10.1088/0960-1317/19/2/025004
27. Liao Y-S, Chen S-T, Lin C-S, Chuang T-J (2005) Fabrication of high aspect ratio microstructure arrays by micro reverse wire-EDM. J Micromech Microeng 15(8):1547–1555. https://doi.org/10.1088/0960-1317/15/8/024
28. Mahapatra SS, Patnaik A (2007) Optimization of wire electrical discharge machining (WEDM) process parameters using Taguchi method. Int J Adv Manuf Technol 34(9-10):911–925. https://doi.org/10.1007/s00170-006-0672-6
29. Roy RK (2001) Design of experiments using the Taguchi approach: 16 steps to product and process improvement. Wiley, New York ISBN: 978-0-471-36101-5
30. Ramakrishnan R, Karunamoorthy L (2006) Multi response optimization of wire EDM operations using robust design of experiments. Int J Adv Manuf Technol 29(1-2):105–112. https://doi.org/10.1007/s00170-004-2496-6
31. Lalchhuanvela H, Doloi B, Bhattacharyya B (2013) Analysis on profile accuracy for ultrasonic machining of alumina ceramics. Int J Adv Manuf Technol 67(5-8):1683–1691. https://doi.org/10.1007/s00170-012-4601-6
32. Singha R, Khamba JS (2008) Comparison of slurry effect on machining characteristics of titanium in ultrasonic drilling. J Mater Process Technology 197:200–205